www.ietdl.org

Published in IET Image Processing
Received on 30th July 2013
Accepted on 23rd February 2014
doi: 10.1049/iet-ipr.2014.0040

ISSN 1751-9659

Edge preservation image enlargement and enhancement method based on the adaptive Perona–Malik non-linear diffusion model

Baraka Maiseli[1,2†], Ogada Elisha[3,4†], Jiangyuan Mei[1], Huijun Gao[1]

[1]*Department of Control Science and Engineering, Research Institute of Intelligent Control and Systems, Harbin Institute of Technology, Harbin 150001, People's Republic of China*
[2]*Department of Electronics and Telecommunication Engineering, University of Dar es Salaam, College of Information and Communication Technology, PO Box 35194, Dar es Salaam, Tanzania*
[3]*Department of Mathematics, Harbin Institute of Technology, Harbin 150001, People's Republic of China*
[4]*Department of Mathematics, Egerton University, PO Box 536, Egerton, Kenya*
[†]*These two authors contributed equally to this work.*
E-mail: barakamaiseli@yahoo.com

Abstract: In this study, the authors have proposed a new super resolution (SR) model based on the Perona–Malik regularisation scheme. The new model integrates into its regularisation component an adaptive exponential term which automatically adjusts itself depending on the local image features. This lends more sensitivity and adaptability to the proposed model, thereby making the reconstruction process much less punishing against semantically important features. Therefore, regularisation is stronger in homogeneous regions, and weaker in the neighbourhood of boundaries. The proposed method has a promising capability of supressing noise more effectively, while preserving important image features. The approach used differs significantly from the available methods, especially in the manner in which adaptability has been deployed. Noting that SR methods are less sensitive to the local image topography, a factor that causes the super-resolved images to be visually poor, the new method sensitively probes the local features of the image, and determines the necessary level of reconstruction and regularisation. Additionally, the formulation robustly introduces a backward diffusion, a phenomenon proved from literature to have a tendency of sharpening edges. The authors have included empirical reconstruction results to demonstrate that their model produces better images in comparison with other classical methods.

1 Introduction

Generally, images can be classified into two categories on the basis of the amount of information they contain, namely high resolution (HR) and low resolution (LR) images. The type of resolution that is referred to in this context is called spatial resolution, and therefore HR images are characterised by having larger number of pixels and more details than LR images. In the field of image processing, HR images are often required for two basic reasons. First, the signal content in the HR images is higher in comparison with the LR images, and this makes them useful in further signal processing in digital systems. Second, human beings are naturally acquainted with better quality images which have appreciable visual appeal [1, 2].

Given an undesirable LR image, there are two main approaches one can use to increase its resolution. The first approach involves increasing the incident surface area of the imaging device sensors. This can be achieved through reducing the size of the pixels of the sensors. There is, however, the maximum sensor density limit which can be achieved, beyond which the imaging system may introduce undesirable features to the output images [3]. This approach is not cost-effective, because it requires hardware modifications. In addition, the approach increases the weight of the imaging device, which may result in challenges in respect of certain imaging applications which require lighter imaging hardware devices, such as in remote sensing applications. These challenges are solved by the second approach, where signal processing techniques are used to improve the resolution of the low-quality images. The technology that implements this strategy is called SR.

SR is one of typical examples of inverse problems which occur in nature (see [3–14], and references therein). It deals with estimation of a HR image from at least one observed LR image. This problem is ill-posed, and therefore appropriate regularisation methods are usually required to counter ill-posedness. For this reason, various forms of regularising functions have been proposed in the literature.

In [15], total variation (TV) regulariser proposed in [16], along with the Bregman iteration algorithm proposed in [17, 18], are used to solve a SR problem. This method provides better results particularly in the aspect of edge recovery. However, the images generated suffer from stair-casing effects. The problem originates with the formulation of the TV model, which favours piecewise constant solutions. This causes smooth regions of the image to be processed into piecewise constant regions; hence the staircase-like features [19, 20].

Farsiu *et al.* [8] proposed a regularisation approach which incorporates the ℓ_1-norm minimisation and the bilateral prior. An important advantage of this method is its robustness to errors caused by motion and blur estimations. In addition, edges in the reconstructed images are relatively sharper. In spite of these merits, the ℓ_1 + bilateral TV method has a tendency to introduce unnecessary features into the output images. Furthermore, the method does not perform well when the input images are contaminated by impulse noise. This drawback is caused by the failure of the photometric function in the bilateral filter to efficiently process the impulse noise value (see [21]).

Kim *et al.* [22] proposed a regularisation function to solve a SR problem using the Perona–Malik (PM) non-linear diffusion model (see [23–25]). One important advantage of this SR method is its capability to preserve crucial image characteristics, particularly edges and contours. However, the method is not sufficiently adaptive; in a sense that the regularisation process is done not on the basis of the variations of the local structural properties of the image, such as textures and other similarly small-scale features.

Gilboa *et al.* proposed a SR method based on the forward-and-backward non-linear diffusion process in [26, 27]. The method uses the diffusion coefficient with parameters k_f (forward coefficient), k_b (backward coefficient) and ω (tuning constant), which can be adaptively updated according to the local image features. Our analysis on this method recognised that there are no automatic mechanisms to adjust the k_f, k_b and ω parameters during the reconstruction process. Therefore some values which possibly would yield optimal results are selected. Obviously, one can see that the manual selection of the activity parameters is tedious and takes time. Besides, with such a multiplicity of parameters, none of which is dynamically determined, obtaining a permutation that yields optimal results remains an arduous challenge.

Recently, Bayesian approaches which are based on the variational methods have been proposed in [28–30]. These Bayesian approaches reveal a problem of being computationally expensive, and the super-resolved images, for certain types of input images, contain spurious new features. As it will be demonstrated later in the subsequent subsections, the super-resolved images by these methods are overly brightened, and this causes loss of naturalness.

The PM scheme in [23] has been applied to solve several problems. Some of the imaging areas that have gained the benefits of this formulation are image denoising, image segmentation and image in painting. The main reason for the widespread application of the PM model is its promising ability to regularise images while preserving and enhancing fine image details. In restoration problems, for instance, the PM model does noise suppression in images while maintaining their important details. However, there are not enough literature regarding the application of this model and its variants in the SR field. In this work, therefore an SR model based on the PM formulation is proposed. Owing to the insufficient ability of the PM formulation to regularise images on the basis of their local features, we introduce an adaptive exponential term in its kernel part. This variable component automatically adjusts the reaction of the diffusion process according to the local structures of an image. The proposed method is adaptive to the effect that it performs reconstruction while providing an automatic interplay between the linear isotropic diffusion and the PM scheme in the regularisation process.

In comparison with other classical SR methods, our method provides some additional advantages. One, the method is computationally efficient, and therefore, it may be ideal when coded into the target boards. Secondly, reconstructed images are visually sharper and contain more useful (detailed) information. In addition, the adaptive nature of the method makes it flexible and robust in a variety of images. Other models are limited to particular types of images because they treat the image features indiscriminately.

The organisation of the remainder of the paper is as follows: in Section 2, the proposed method is detailed. Discussion on the experimental results is done in Section 3 and Section 4 concludes the paper.

2 G-PMSR method

In this section, we propose an SR model, called the Gamma-Perona Malik super resolution (G-PMSR), which is based on the PM framework to perform the reconstruction process. The new model has a variable exponent, $\gamma(z)$, which adaptively adjusts itself according to the local image characteristics. In regions of the image where the magnitude of the gradient is high, indicating areas of likely to have edge, the value of $\gamma(z)$ approaches 2, thereby allowing the regularisation term take the PM formulation. This allows the proposed formulation to preserve edges. However, in homogeneous regions, where the magnitude of the gradient is small, $\gamma(z)$ approaches 0. In this case, the proposed method favours the linear isotropic diffusion, thereby allowing smoothing away of noise. The model adopts variants of it for $0 < \gamma(z) < 2$ that make it have a higher sensitivity that allows it to preserve finer details of the image.

Therefore we propose a SR method which combines the evolution equation from a variational problem

$$\inf_u \left\{ P(u) = \frac{1}{2K} \sum_{k=1}^{K} \| y_k - \boldsymbol{W}_k \boldsymbol{B}_k \boldsymbol{D}_k u \|_2^2 \right\} \qquad (1)$$

where u is the HR image being sought, y_k stands for the observed sequence of LR images, $\boldsymbol{W}_k$, $\boldsymbol{B}_k$ and $\boldsymbol{D}_k$ are operators which represent warping, blurring and decimation matrices, respectively, in a degradation observation model of the imaging system and an elliptic partial differential equation regularisation problem

$$0 = \beta_1 \nabla . \left(\frac{\nabla u}{\left(1 + [|\nabla u|/\lambda]^{\gamma(z)}\right)} \right) - \beta_2 (u - u_o) \qquad (2)$$

where β_1 is a regularising parameter, β_2 is a fidelity forcing threshold parameter and $0 \le \gamma(z) \le 2$. From (1), we derive

IET Image Process., 2014, Vol. 8, Iss. 12, pp. 753–760
doi: 10.1049/iet-ipr.2014.0040

the corresponding Euler–Lagrange equation given as

$$0=\frac{1}{K}\sum_{k=1}^{K}(\boldsymbol{W}_k^{\mathrm{T}}\boldsymbol{B}_k^{\mathrm{T}}\boldsymbol{D}_k^{\mathrm{T}}(\boldsymbol{W}_k\boldsymbol{B}_k\boldsymbol{D}_k u-y_k)) \quad (3)$$

Now, combining (2) and (3) and embedding the result into a time-marching system, we obtain the following evolution equation

$$\frac{\partial u}{\partial t}=\sum_{k=1}^{K}(\boldsymbol{W}_k^{\mathrm{T}}\boldsymbol{B}_k^{\mathrm{T}}\boldsymbol{D}_k^{\mathrm{T}}(\boldsymbol{W}_k\boldsymbol{B}_k\boldsymbol{D}_k u-y_k)) + \beta_1 K\nabla.\left(\frac{\nabla u}{(1+[|\nabla u|/\lambda]^{\gamma(z)})}\right)-\beta_2\, K(u-u_o) \quad (4)$$

The variable component $\gamma(z)$ in (4) automatically and adaptively adjusts the regularisation part on the basis of the local image structures. Let

$$Q_{\mathrm{SR}}(u)=\sum_{k=1}^{K}(\boldsymbol{W}_k^{\mathrm{T}}\boldsymbol{B}_k^{\mathrm{T}}\boldsymbol{D}_k^{\mathrm{T}}(\boldsymbol{W}_k\boldsymbol{B}_k\boldsymbol{D}_k u-y_k))$$

and

$$R(u)=\beta_2\, K(u_o-u)$$

Then, it can easily be seen that, when $\gamma(z)=0$, the evolution equation becomes

$$\frac{\partial u}{\partial t}=Q_{\mathrm{SR}}(\cdot)+\beta_1\, K\Delta u+R(\cdot) \quad (5)$$

in which case the regularisation process favours homogeneous parts of the image. When $\gamma(z)=1$ we obtain an evolution equation

$$\frac{\partial u}{\partial t}=Q_{\mathrm{SR}}(\cdot)+\beta_1 K\nabla.\left(\frac{\nabla u}{(1+[|\nabla u|/\lambda])}\right)+R(\cdot) \quad (6)$$

which has a regularisation part similar to Charbonnier formulation in [31]. In addition, for $\gamma(z)=2$, the evolution equation becomes

$$\frac{\partial u}{\partial t}=Q_{\mathrm{SR}}(\cdot)+\beta_1 K\nabla.\left(\frac{\nabla u}{(1+[|\nabla u|/\lambda]^2)}\right)+R(\cdot) \quad (7)$$

which is the SR model based on the PM scheme. Observe that, in each of (5), (6) and (7), $Q_{\mathrm{SR}}(\cdot)$ and $R(\cdot)$, respectively, are resolution and fidelity parts of the proposed model. It is, however, desirable to make $\gamma(z)$ self-adjusting during the iteration process. After several experiments, we found that

$$\gamma(z)=2(1-\kappa\exp(-|G_\sigma * u|)) \quad (8)$$

where $\kappa\in[0, 1]$ is a tuning parameter and G_σ is a Gaussian kernel, was suitable for our purpose.

Finally, we give explanations on how the proposed method is capable of preserving edges. Consider Fig. 1 below, representing a contour (isophote line) S in an image u. The variables u_{NN} and u_{TT} are defined in (9). The components

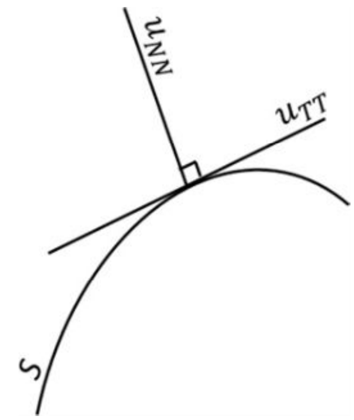

Fig. 1 *Tangent and normal components on isophote lines*

$\boldsymbol{N}(x)$ and $\boldsymbol{T}(x)$ given in (10) represent the normal and tangent vectors to S, respectively.

$$\begin{aligned} u_{\mathrm{TT}}&=T'\nabla^2 uT=\frac{1}{|\nabla u|^2}(u_x^2u_{yy}+u_y^2u_{xx}-2u_xu_yu_{xy})\\ u_{\mathrm{NN}}&=N'\nabla^2 uN=\frac{1}{|\nabla u|^2}(u_x^2u_{xx}+u_y^2u_{yy}+2u_xu_yu_{xy})\end{aligned} \quad (9)$$

$$\begin{aligned}\boldsymbol{N}(x)&=\nabla u/|\nabla u|\\ \boldsymbol{T}(x)&=(-u_y, u_x)/|\nabla u|\end{aligned} \quad (10)$$

Finally, we show the behaviour of our proposed model, particularly on the aspect of performing reconstruction while adaptively regularising the image. Therefore we first expand (4) to obtain

$$\frac{\partial u}{\partial t}=Q_{\mathrm{SR}}(\cdot)+\beta_1 K\nabla_x\left(\frac{u_x}{\left(1+\left[\sqrt{u_x^2+u_y^2}/\lambda\right]^{\gamma(z)}\right)}\right) + \beta_1 K\nabla_y\left(\frac{u_y}{\left(1+\left[\sqrt{u_x^2+u_y^2}/\lambda\right]^{\gamma(z)}\right)}\right)+R(\cdot) \quad (11)$$

If we further simplify (11) and substitute where necessary the u_{TT} and u_{NN} components, as defined in (9), we obtain

$$\frac{\partial u}{\partial t}=Q_{\mathrm{SR}}(\cdot)+\beta_1\, K\left(\frac{1}{1+[|\nabla u|/\lambda]^{\gamma(z)}}\right)u_{\mathrm{TT}} + \beta_1\, K\left(\frac{1+(1-\gamma(z))\,[|\nabla u|/\lambda]^{\gamma(z)}}{\left(1+[|\nabla u|/\lambda]^{\gamma(z)}\right)^2}\right)u_{\mathrm{NN}}+R(\cdot) \quad (12)$$

where (12) basically represents the decomposition of (4) into tangent (T) and normal (N) directions to the isophote lines. Observe from (12) that, as $|\nabla u|\to 0$, signifying homogeneous regions, the regularisation becomes uniform (linear isotropic diffusion). Furthermore, as $|\nabla u|\to+\infty$, signifying availability of an edge, the u_{NN} components diminish at a faster rate than the u_{TT} components. Consequently, important features like textures and edges are

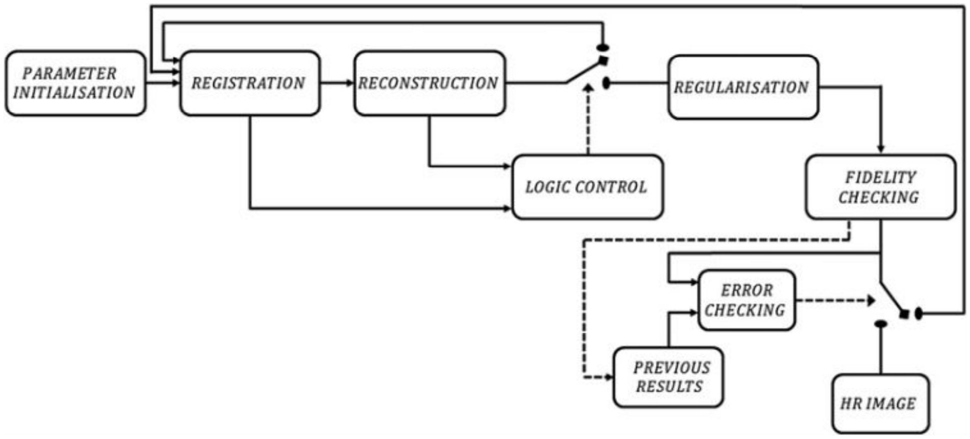

Fig. 2 *SR regularisation model*

preserved. Another advantage of the formulation is its ability to allow backward diffusion, which has a tendency to sharpen edges. The condition for the backward diffusion is

$$\frac{|\nabla u|}{\lambda} < \left(\frac{1}{\gamma(z) - 1}\right)^{1/\gamma(z)} \tag{13}$$

The proposed block diagram which can be used to implement the G-PMSR method is shown in Fig. 2.

3 Experimental results and discussion

3.1 Setup of the experiments

Using a Compaq610 computer, having Intel(R) Core(TM)2 Duo CPU T5870 each 2.00 GHz, physical RAM of 2.00 GB and Professional Windows 7 64-bit operating system, four regions of interest (ROIs), namely ROI-1, ROI-2, ROI-3 and ROI-4, were extracted from a HR image of an elephant (see Fig. 3). In additionally, two ROIs, namely ROI-5 and ROI-6, were extracted from a HR image of a pot (see Fig. 4). The ROIs after being extracted from the HR images are shown in Fig. 5. Furthermore, the corresponding sequences of LR images from each of the ROIs were generated (see the illustration in Fig. 6). Finally, super-resolved images were generated from the given LR image sequences using the methods ℓ_1-SAR in [30], TV-SR in [28], ℓ_1-SR in [29] and G-PMSR. The software used for generating the hyper-resolved images of the other methods was taken from [32], and the registration method proposed in [33] was used in our method to estimate the motion parameters. Some of the results for the reconstructed images using these methods are demonstrated in Fig. 7.

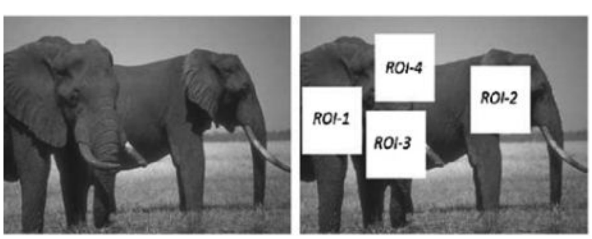

Fig. 3 *Left: HR image of an elephant, right: HR image of an elephant containing different ROIs*

3.2 Discussion of the experimental results

The performance evaluation of the methods was done using the experimental results obtained in the Section 3.1. The subjective assessment shows that, the visual appeal of the HR images produced by our method is better in relation to other methods. The images produced by the G-PMSR method (see Fig. 7) are sharper and more natural. The other methods show a tendency of producing images which are relatively blurred, out of focus and poor in contrast.

Using the quantitative measures, the proposed method generates images having higher values of the peak signal-to-noise ratio (PSNR). This signifies higher signal contents in the super-resolved images compared with other methods. Furthermore, the G-PMSR method offers low root mean square error (RMSE) [34] values in the final reconstructed images. The PSNR and RMSE values for different methods are illustrated in Table 1. The graphs in Fig. 8 provide a quick observation of the performance of the G-PMSR method.

In Fig. 9, similarity plots between the result produced by each of the considered methods and the ideal HR image are given. Clearly, it is observable that the plot of our method traces more closely the ideal curve. This indicates higher degree of similarity between the reconstructed image and the original image.

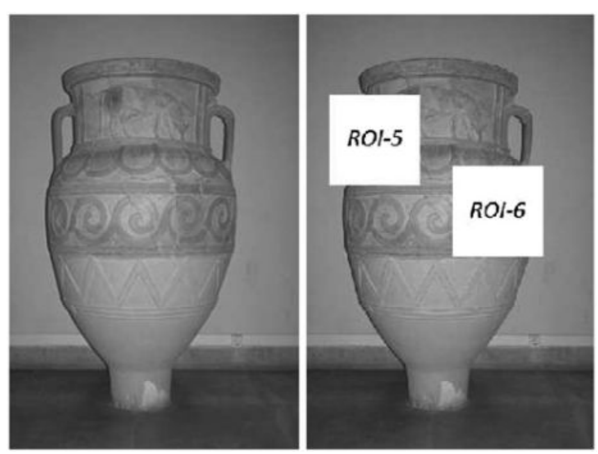

Fig. 4 *Left: HR image of a pot, right: HR image of a pot containing different ROIs*

IET Image Process., 2014, Vol. 8, Iss. 12, pp. 753–760
doi: 10.1049/iet-ipr.2014.0040

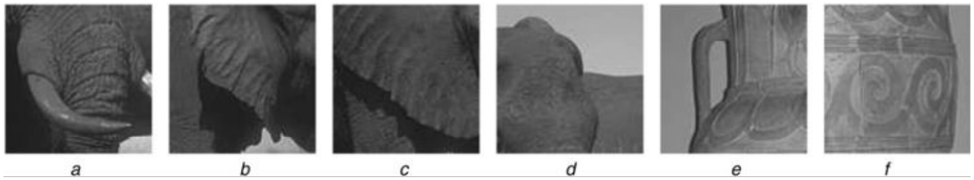

Fig. 5 *Different ROIs of the HR images of a pot and an elephant*
a ROI-1
b ROI-2
c ROI-3
d ROI-4
e ROI-5
f ROI-6

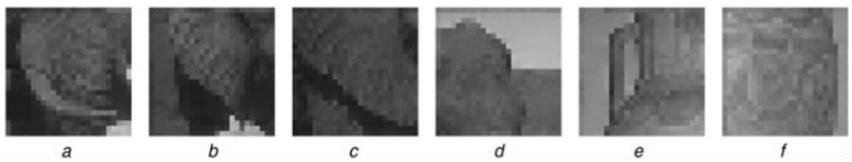

Fig. 6 *One of the LR images generated from the corresponding ROIs (× 2.0)*
a LR from ROI-1
b LR from ROI-2
c LR from ROI-3
d LR from ROI-4
e LR from ROI-5
f LR from ROI-6

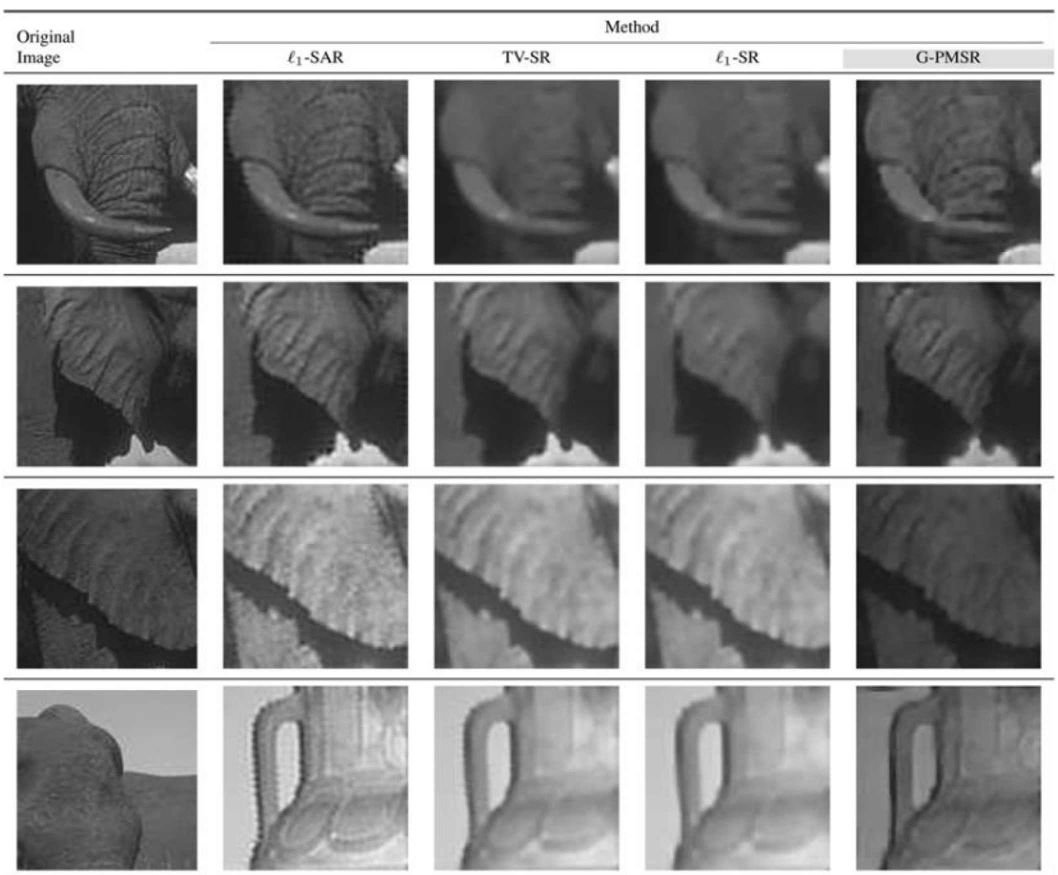

Fig. 7 *Results of SR for various methods*

Table 1 Image quality comparison results table

Image	Method							
	ℓ_1-SAR		TV-SR		ℓ_1-SR		G-PMSR	
	PSNR	RMSE	PSNR	RMSE	PSNR	RMSE	PSNR	RMSE
ROI-1	20.7893	23.2849	20.7690	23.3394	20.5805	23.8515	24.6970	14.8488
ROI-2	20.1233	25.1407	20.0788	25.2696	20.0082	25.4759	24.7785	14.7102
ROI-3	10.5051	76.0826	10.5098	76.0413	10.5005	76.1230	27.9397	10.2224
ROI-4	16.6140	37.6566	16.5783	37.8117	16.4593	38.3332	23.6147	16.8191
ROI-5	12.9217	57.6045	12.8997	57.7502	12.7502	58.7529	21.8524	20.6025
ROI-6	15.1183	44.7326	15.0865	44.8968	15.0540	45.0651	21.1051	22.4535
mean	16.0120	44.0837	15.9870	44.1848	15.8921	44.6003	23.9979	16.6094
STD	4.0190	20.1985	4.0075	20.1608	3.9721	20.1481	2.4394	4.4191
ranking	2	2	3	3	4	4	1	1

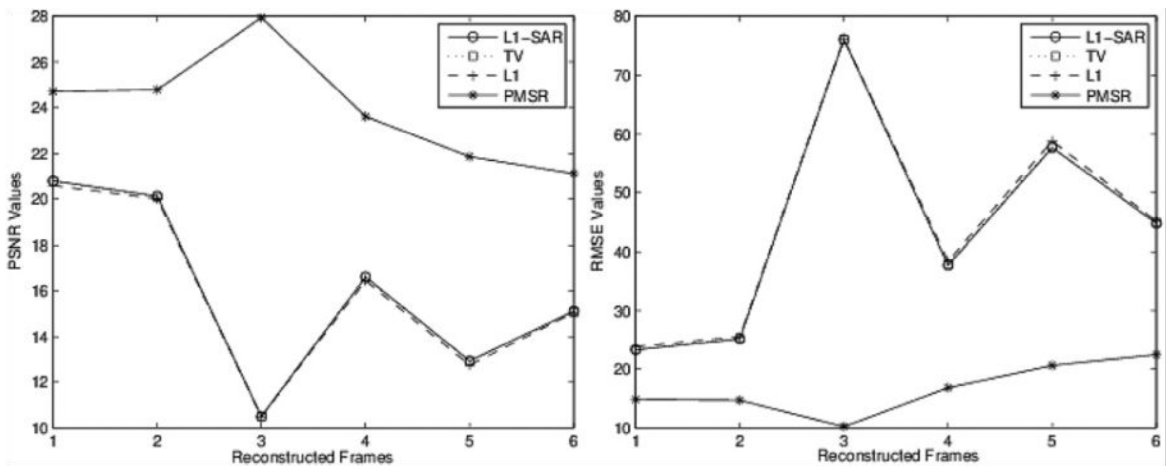

Fig. 8 *Left: PSNR against ROIs, right: RMSE against ROIs*

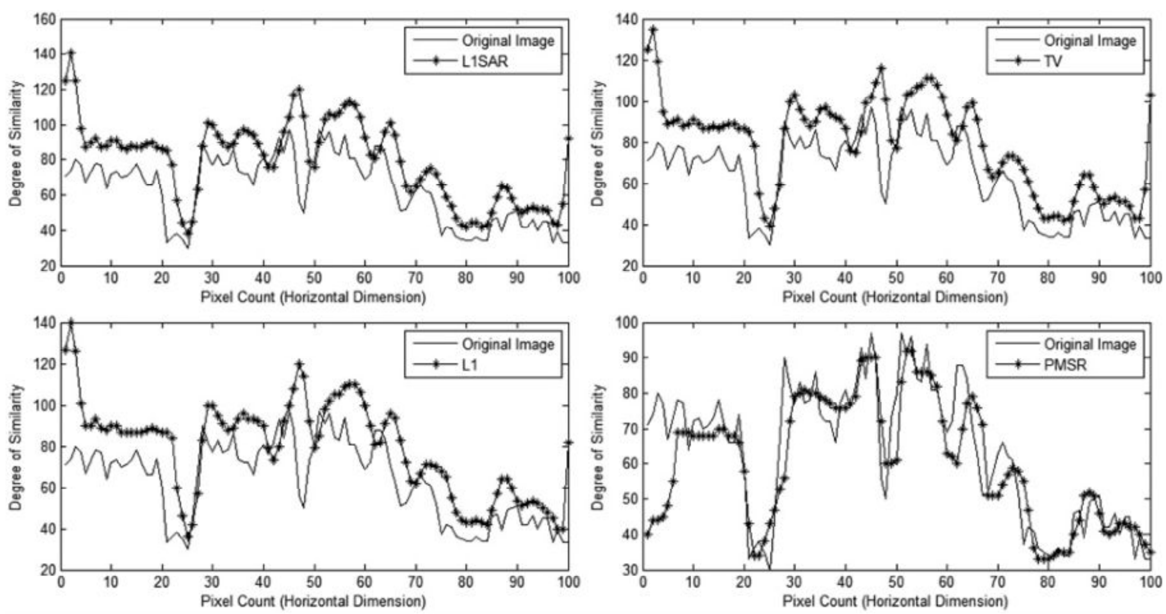

Fig. 9 *Similarity measures for various methods*

doi: 10.1049/iet-ipr.2014.0040

Table 2 Computational efficiency evaluation table

Image	CPU Time (seconds) (τ)			
(r)2-5	ℓ_1-SAR	TV-SR	ℓ_1-SR	G-PMSR
ROI-1	221.2213	483.6800	714.2360	7.7896
ROI-2	212.8022	628.8581	849.2174	8.8572
ROI-3	335.5963	444.8306	601.3076	7.2410
ROI-4	279.3851	600.4759	782.9267	7.2290
ROI-5	234.7593	548.5098	739.7428	12.1297
ROI-6	210.3722	321.0743	465.3308	9.6569
mean	249.0227	504.5715	692.1269	8.8172
speed	$\tau/28$	$\tau/57$	$\tau/78$	τ

There are reasons for the proposed approach to generate visually appreciable images having higher PSNR values and lower RMSE values. In Section 2, a mathematical presentation of the coupling between the normal and tangential components in the proposed regularising kernel [see (12)] is provided. One should note that these two components are responsible in determining the effectiveness of regularisation. Our formulation has ensured a proper balance and interplay of the mentioned components. Moreover, the added capacity of the G-PMSR method to, adaptively, introduce a backward–forward [see (13)] enhances the sharpness of the edges. As a matter of emphasis, the ability of the model to take several variants of it for $0 < \gamma(z) < 2$ makes it be more responsive. This attribute allows it to recover, sharpen and preserve finer details of the image; hence the clarity of the images.

Another performance index, which was used to evaluate the methods, is the computational load. Table 2 demonstrates the numerical values of the CPU running times for the ℓ_1-SAR, TV, ℓ_1-SR and G-PMSR methods. From the table, the G-PMSR method is ×28, ×57 and ×78, faster than the methods ℓ_1-SAR, TV and ℓ_1-SR, respectively. The graph illustrated in Fig. 10 further demonstrates that the proposed method is computationally inexpensive.

The observed high execution speed of the G-PMSR method can well be explained from its implementation algorithm. In the implementation of the evolution (7), we used a four-point explicit numerical scheme with a time step of $\tau \le 0.25$ in conformance with the Courant–Friedrichs–Lewy criterion in [35]. This condition guarantees stability and relatively higher processing speeds. Moreover, our algorithm directly used the scheme without decomposing the regularisation part of (4) into its corresponding partial derivatives. This considerably minimised the number of multiply–add operations. Consequently, the overall execution speed improved.

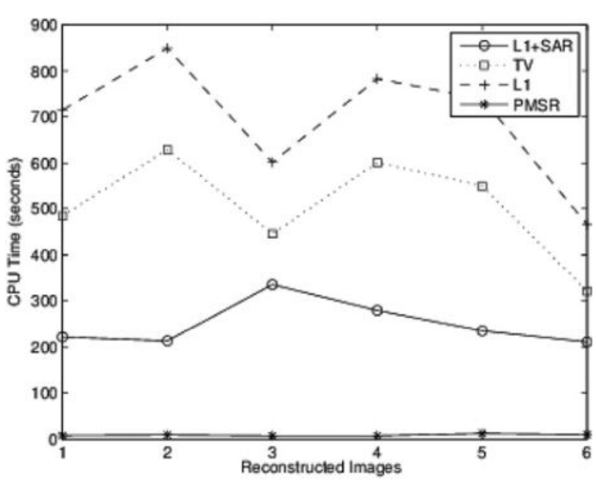

Fig. 10 *Processing times of the algorithms*

4 Conclusion

In this research work, a SR method, which is capable of reconstructing high-quality images from low quality and noisy images, is proposed. A number of experiments presented in the paper demonstrate the capability of the method to emphasise crucial image characteristics, especially edges and contours. The method proposed enhances visual naturalness of the output images. In addition, it makes the reconstructed images clearer and sharper, as illustrated from the summary of the experimental results. As part of future work, we intend to embed this method into the real digital signal processor hardware. The promising higher computational efficiency the proposed method has implies that we may achieve considerably high performance when the new algorithm is embedded into the real hardware platforms.

5 References

1 Kang, M.G., Chaudhuri, S.: ‘Super-resolution image reconstruction’, *IEEE Signal Process. Mag.*, 2003, **20**, (3), pp. 19–20
2 Yang, Q., Yang, R., Davis, J., Nistér, D.: ‘Spatial-depth super resolution for range images’. IEEE Conf. Computer Vision and Pattern Recognition, 2007 (CVPR’07), 2007, pp. 1–8
3 Park, S.C., Park, M.K., Kang, M.G.: ‘Super-resolution image reconstruction: a technical overview’, *IEEE Signal Process. Mag.*, 2003, **20**, (3), pp. 21–36
4 Maalouf, A., Larabi, M.-C.: ‘Image super-resolution, a state-of-the-art review and evaluation’. Advanced Color Image Processing and Analysis, 2013, pp. 181–218
5 Hardeep, P., Swadas, P.B., Joshi, M.: ‘A survey on techniques and challenges in image super resolution reconstruction’, *Int. J. Comput. Sci. Mob. Comput.*, 2013, **2**, pp. 317–325
6 Yang, M., Wang, Y.: ‘A self-learning approach to single image super-resolution’, *IEEE Trans. Multimed.*, 2013, **15**, pp. 498–508
7 Li, X., Hu, Y., Gao, X., Tao, D., Ning, B.: ‘A multi-frame image super-resolution method’, *Signal Process.*, 2010, **90**, (2), pp. 405–414
8 Farsiu, S., Robinson, M.D., Elad, M., Milanfar, P.: ‘Fast and robust multiframe super resolution’, *IEEE Trans. Image Process.*, 2004, **13**, (10), pp. 1327–1344
9 Tao, D., Zhang, K., Gao, X., Li, X.: ‘Single image super-resolution with non-local means and steering kernel regression’, *IEEE Trans. Image Process.*, 2012, **21**, pp. 4544–4556
10 Gao, X., Zhang, K., Tao, D., Li, X.: ‘Image super-resolution with sparse neighbor embedding’, *IEEE Trans. Image Process.*, 2012, **21**, (7), pp. 3194–3205
11 Tang, Y., Yan, P., Yuan, Y., Li, X.: ‘Single-image super-resolution via local learning’, *Int. J. Mach. Learn. Cybern.*, 2011, **2**, (1), pp. 15–23
12 Maiseli, B., Wu, C., Mei, J., Liu, Q., Gao, H.: ‘A robust super-resolution method with improved high-frequency components estimation and aliasing correction capabilities’, *J. Franklin Inst.*, 2014, **351**, (1), pp. 513–527
13 Maiseli, B.J., Liu, Q., Elisha, O.A., Gao, H.: ‘Adaptive Charbonnier superresolution method with robust edge preservation capabilities’, *J. Electron. Imaging*, 2013, **22**, (4), pp. 043027–043027
14 Tang, Y., Yuan, Y., Yan, P., Li, X.: ‘Greedy regression in sparse coding space for single-image super-resolution’, *J. Vis. Commun. Image Represent.*, 2013, **24**, (2), pp. 148–159
15 Marquina, A., Osher, S.J.: ‘Image super-resolution by TV-regularization and Bregman iteration’, *J. Sci. Comput.*, 2008, **37**, (3), pp. 367–382
16 Rudin, L.I., Osher, S., Fatemi, E.: ‘Nonlinear total variation based noise removal algorithms’, *Physica D, Nonlinear Phenom.*, 1992, **60**, (1), pp. 259–268
17 Goldstein, T., Osher, S.: ‘The split Bregman method for l1-regularized problems’, *SIAM J. Imaging Sci.*, 2009, **2**, (2), pp. 323–343

18 Getreuer, P.: 'Rudin-Osher-Fatemi total variation denoising using split Bregman', *IPOL*, 2012, **10**, pp. 74–95
19 Chen, Y., Levine, S., Rao, M.: 'Variable exponent, linear growth functionals in image restoration', *SIAM J. Appl. Math.*, 2006, **66**, (4), pp. 1383–1406
20 Chen, Y., Rao, M.: 'Minimization problems and associated flows related to weighted p energy and total variation', *SIAM J. Math. Anal.*, 2003, **34**, (5), pp. 1084–1104
21 Huang, Y.-L., Fuh, C.-S.: 'Noise reduction using enhanced bilateral filter', *Images Recognit.*, 2006, **12**, (4), pp. 46–53
22 Kim, H., Jang, J.-H., Hong, K.-S.: 'Edge-enhancing super-resolution using anisotropic diffusion'. Proc. 2001 Int. Conf. Image Processing, 2001, 2001, vol. 3, pp. 130–133
23 Perona, P., Malik, J.: 'Scale-space and edge detection using anisotropic diffusion', *IEEE Trans. Pattern Anal. Mach. Intell.*, 1990, **12**, (7), pp. 629–639
24 Kichenassamy, S.: 'The Perona–Malik paradox', *SIAM J. Appl. Math.*, 1997, **57**, (5), pp. 1328–1342
25 Perona, P., Shiota, T., Malik, J.: 'Anisotropic diffusion'. Geometry-Driven Diffusion in Computer Vision, 1994, pp. 73–92
26 Gilboa, G.: 'Super-resolution algorithms based on inverse diffusion-type processes' PhD thesis, Technion-ISrael InStitute of Technology, 2004
27 Gilboa, G., Sochen, N., Zeevi, Y.Y.: 'Forward-and-backward diffusion processes for adaptive image enhancement and denoising', *IEEE Trans. Image Process.*, 2002, **11**, (7), pp. 689–703
28 Babacan, S., Molina, R., Katsaggelos, A.K.: 'Variational Bayesian super resolution', *IEEE Trans. Image Process.*, 2011, **20**, (4), pp. 984–999
29 Villena, S., Vega, M., Molina, R., Katsaggelos, A.K.: 'Bayesian super-resolution image reconstruction using an l1 prior'. IEEE Proc. Sixth Int. Symp. Image and Signal Processing and Analysis, 2009 (ISPA 2009), 2009, pp. 152–157
30 Villena, S., Vega, M., Babacan, S.D., Molina, R., Katsaggelos, A.K.: 'Bayesian combination of sparse and non sparse priors in image super resolution', *Digit. Signal Process.*, 2012, **23**, pp. 530–541
31 Charbonnier, P., Blanc-Feraud, L., Aubert, G., Barlaud, M.: 'Two deterministic half-quadratic regularization algorithms for computed imaging'. IEEE Proc. Int. Conf. Image Processing, 1994 (ICIP-94), 1994, vol. 2, pp. 168–172
32 Superresolution software. http://decsai.ugr.es/pi/superresolution/software.html, 2012, accessed 29 February 2013
33 Irani, M., Peleg, S.: 'Improving resolution by image registration', *CVGIP, Graph. Models Image Process.*, 1991, **53**, (3), pp. 231–239
34 Wang, Z., Bovik, A.C.: 'Mean squared error: love it or leave it? A new look at signal fidelity measures', *IEEE Signal Process. Mag.*, 2009, **26**, (1), pp. 98–117
35 Courant, R., Friedrichs, K., Lewy, H.: 'On the partial difference equations of mathematical physics', *IBM J. Res. Dev.*, 1967, **11**, (2), pp. 215–234

doi: 10.1049/iet-ipr.2014.0040